ROYAL SOCIETY
OF CHEMISTRY

PAPER

Check for updates

Liquid exfoliation of a series of expanded layered Cu(II)-paddlewheel metal–organic frameworks to form nanosheets†

Joshua Nicks, (ID) Thomas M. Roseveare, (ID) Michael S. Harris, (ID)
David J. Ashworth, (ID) George Danczuk, Lee Brammer (ID) and Jonathan A. Foster (ID) *

Ultrasonic liquid exfoliation provides a convenient route for converting layered materials into nanosheets. However, the relationship between the structure and morphology of the bulk materials and the properties of the resulting nanosheets remains poorly understood. In this work, we prepare an isoreticular series of layered metal–organic frameworks (MOFs) based on linear aromatic dicarboxylate derivatives (L1, L2, L3) with three different linker lengths (L3 > L2 > L1) and using copper(II) nitrate and acetate as metal ion sources. Liquid exfoliation of large crystals of all three MOFs [$Cu_2(L)_2$](solvent)$_2$, synthesised from $Cu(NO_3)_2$, produced monolayer nanosheets with longer linkers leading to larger lateral dimensions. Exfoliation of smaller MOF crystals, formed using the copper(II) acetate salt under identical conditions, produced a much higher concentration of multi-layer nanosheets with smaller lateral dimensions. These results indicate that the initial crystal size plays an important role in determining both the lateral dimensions and the thicknesses of nanosheets. Such insights contribute to a deeper understanding of the design principles governing metal–organic framework nanosheets (MONs) and other two-dimensional materials.

Introduction

Metal–organic framework nanosheets (MONs) combine the highly tunable structures and properties of other metal–organic materials with the high surface areas and molecular thicknesses associated with other two-dimensional (2D) materials.[1–4] MONs have been shown to outperform their bulk counterparts, metal–organic frameworks (MOFs), in a wide range of sensing, catalysis, electronics and separation applications.[5] The vast number of known MOFs with layered structures has served as an effective starting point for the formation of MONs through "top-down" delamination processes.[6,7]

Ultrasonic liquid exfoliation has been widely applied to a range of different 2D materials, due to its ease of setup and wide applicability.[8,9] Recent work in this field has identified the importance of factors such as the matching of solvent and solute surface tension parameters for the production of ultrathin nanosheets from layered materials.[10–13] In the case of MONs, their modular structure provides a unique opportunity to investigate the effect of systematic changes in the structure of layered materials on the size and properties of the

nanosheets produced.[3,14] Identifying how the properties of layered MOFs affect the process of their exfoliation into nanosheets is vital for understanding how to optimise the design of such materials. Despite this, few studies have examined what factors influence the exfoliation of MOFs including the thicknesses, lateral sizes, and concentrations of the nanosheets obtained.

The majority of work in this area has examined how the use of different solvent systems affects the exfoliation of layered MOFs into MONs. Moorthy *et al.* have probed the degree of exfoliation by correlating the relative fluorescence intensity with nanosheet concentration in suspension, taking a screening approach to investigate the suitability of different solvents as exfoliation media based on their hydrogen-bonding capabilities.[15,16] Yang *et al.* used a mixed methanol/*n*-propanol solvent system to obtain high quality $Zn_2(bim)_4$ nanosheets (bim = benzimidazolate), attributing the enhanced exfoliation to smaller methanol molecules penetrating between the MOF layers, whereas larger *n*-propanol molecules adsorb onto and stabilise the nanosheet surfaces.[17] Reports by Wang *et al.* and Ni *et al.* noted improved exfoliation, in terms of both concentration and aspect ratio, when using ionic liquids as exfoliation media, which stabilise nanosheets during their formation by acting as surfactants.[18,19] A report by Fu and co-workers demonstrated that the introduction of monotopic modulators which reduce epitaxial crystal growth can facilitate the enhanced dispersion of nanosheets.[20] Gosch *et al.* reported a

Department of Chemistry, University of Sheffield, Sheffield, UK.
E-mail: jona.foster@sheffield.ac.uk

†Electronic supplementary information (ESI) available: Full experimental details, including synthetic procedures, exfoliation studies and characterisation methods. See DOI: https://doi.org/10.1039/d4nr02663b

systematic study of the ultrasonic exfoliation of 6 different layered frameworks and found a complex relationship between the crystal structure and ease of exfoliation, but suggested that porosity and polarity could be decisive factors.[21]

In our previous work, we have made use of isoreticular substitution to systematically tune the structure of layered MOFs and understand the effect on their exfoliation to form MONs. We demonstrated that the incorporation of benzenedicarboxylate derivatives with hydrophilic or hydrophobic chain substituents into paddlewheel-based layered MOFs gave rise to significant differences between the two derivatives in both the dispersion properties and the nanoscopic dimensions of the MONs upon exfoliation in solvents of various polarities.[22] Furthermore, mixed-ligand MONs exhibited enhanced exfoliation in both polar and apolar solvents compared to either the hydrophilic or hydrophobic single-ligand MON.[23] Although broad particle size distributions made drawing clear trends challenging, results in another study indicate that in MONs functionalised with alkyl chains of different lengths, shorter chains afforded MONs in the highest concentrations whilst longer chains led to thinner nanosheets with higher surface areas.[24] Blending of these ligands in mixed-ligand MONs demonstrated that alkyl substituents with more disparate chain lengths produced thicker nanosheets than those in which chain lengths closer in length were used.[23] Finally, we have shown how post-synthetic ligand functionalisation can be used to enhance exfoliation into ultrathin nanosheets[25] and tune properties post-exfoliation.[26]

In this work, we investigate two different parameters and their effect on the exfoliation of layered MOFs into nanosheets: (1) isoreticular linker expansion, and (2) the choice of the copper(II) salt used in MOF synthesis. The linker precursors chosen, shown in Fig. 1a, are 1,4-naphthalenedicarboxylic acid (H$_2$(1,4-NDC), L1), 2,6-naphthalenedicarboxylic acid (H$_2$(2,6-NDC), L2), and biphenyl-4,4'-dicarboxylic acid (H$_2$(BPDC), L3). All three linkers contain two aromatic rings but the different connectivities mean they provide different linker lengths. Here we reacted the diacid linker precursors with copper(II) salts to produce an expanded isoreticular series of layered MOFs based on the Cu$_2$(O$_2$CR)$_4$ paddlewheel (PW) secondary building unit. This series therefore provides an ideal opportunity to test the effect of linker length/node spacing on the properties of the nanosheets.
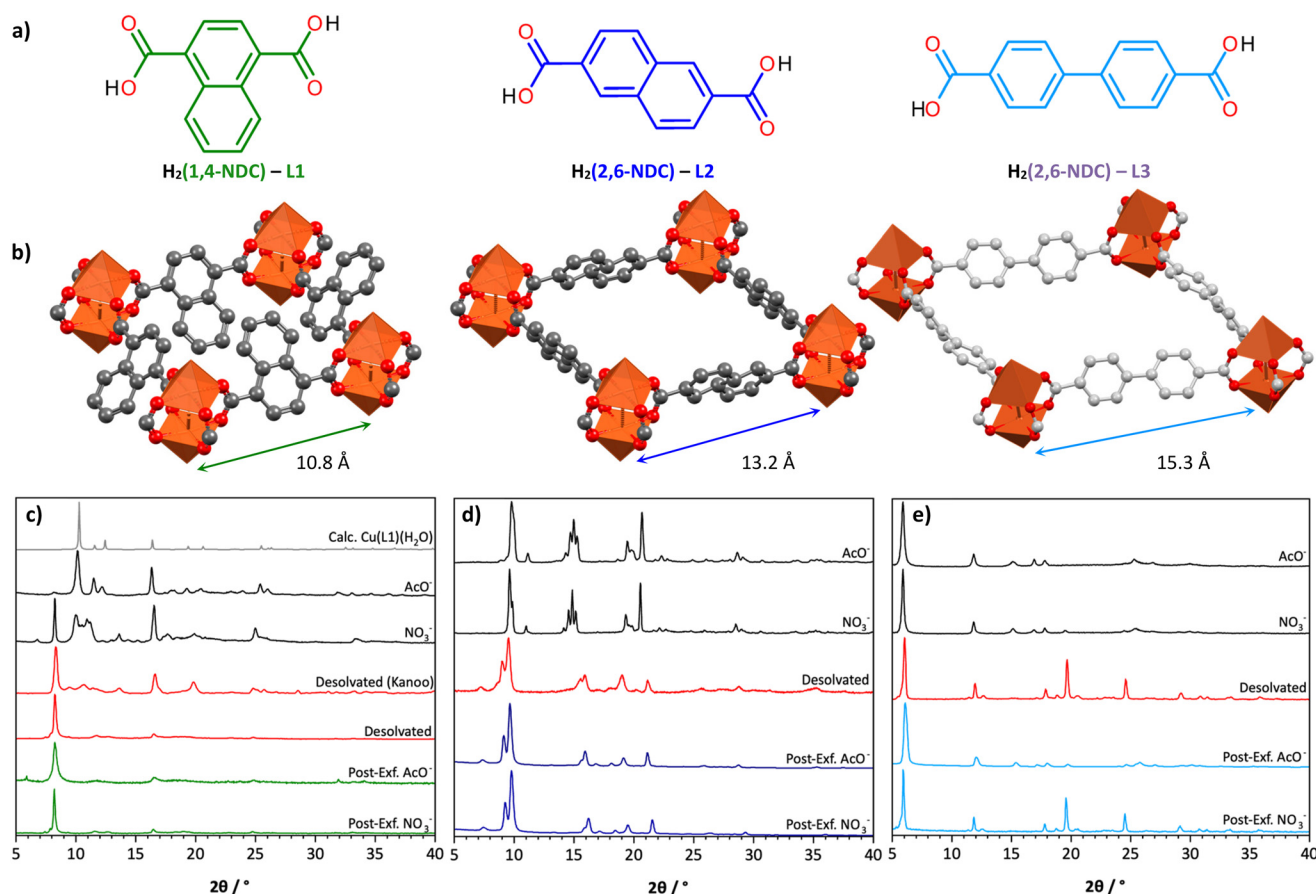

Fig. 1 (a) Structures of the linker precursors, L1, L2, and L3 used in this study. (b) Crystal structure representations of the layers of Cu(L1) (CSD Refcode MAXDEW),[27] Cu(L2) (CSD Refcode XOMBAC)[28] and Cu(L3) (adapted from CSD refcode PURRUQ which has the ligand 3,3'-dimethoxy-4,4'-biphenyldicarboxylate)[29] illustrating the expansion in grid dimensions. Experimental PXRD patterns obtained for the (c) Cu(L1), (d) Cu(L2), and (e) Cu(L3) MOFs synthesised from the nitrate and acetate solvent (black), desolvated with acetonitrile (red), and obtained post–exfoliation (colour coded to linker). Additional literature patterns are provided for the Cu(L1) system.[27]

This series of MOFs were prepared using copper(II) nitrate trihydrate and copper(II) acetate monohydrate. The nitrate salt has a greater solubility in DMF which typically leads to slower crystallisation and large crystallites compared to the acetate salt which pre-organises in the paddlewheel unit (as $Cu_2(O_2CMe)_4$) and facilitates faster deprotonation of the diacid linker precursor resulting in more rapid nucleation and smaller crystallites. Thus, this also provides an opportunity to investigate the effect of the starting MOF crystal size on the resulting nanosheets.

Results and discussion

Synthesis of the isoreticular layered MOF series

All the MOFs were prepared according to the same procedure, in which separate DMF solutions of the chosen copper salt and the protonated linker precursor were combined in glass reaction vials with Teflon-lined caps and heated to 110 °C for 18 hours. After formation, the MOF crystals were washed three times with DMF and diethyl ether to remove the unreacted starting material and excess solvent. Full details of the synthetic procedure can be found in the Experimental section and all data not included in the paper can be found in the ESI.† As we have previously observed loss of co-ordinated solvent molecules to the axial positions of similar Cu_2-PW structures during exfoliation in acetonitrile we sought to characterise these desolvated phases for the isoreticular series prepared in this report.[23,30] Fully desolvated MOFs were obtained by washing the solvated systems with acetonitrile five times before drying. ^{1}H NMR spectroscopy of the digested samples was used to confirm full desolvation for all samples (Section S4†).

Each MOF has a layered structure, in which four dicarboxylate linkers coordinate to Cu_2-PW, interconnecting these units in the **sql** topology. Thus, each structure features strong metal–carboxylate bonding within the layers, and only weak intermolecular interactions between the layers. We have closely examined the structures of these materials through Pawley refinement to determine unit cell parameters via the fitting of PXRD patterns and comparisons with published reports of similar two-dimensional PW structures.[27,28,31–33] Full details of this investigation are given in Section S2† and it is summarised herein.

Cu(L1) forms as a green powder from both salts. Elemental microanalysis and ^{1}H NMR spectroscopy of the digested samples indicate that the MOF prepared from the nitrate source is only 84% solvated by DMF, presumed to be axially co-ordinated to the Cu centres. The acetate synthesised MOF has an excess of DMF present at 126% solvation, attributed to solvent molecules retained in the pores in addition to the co-ordinated DMF. These degrees of solvation are reflected in the PXRD patterns of the MOFs, which can be fitted as a mixture of an $I4/mmm$ major phase and a $Pbcn$ minor phase, both consistent with the single-crystal structures reported by Kanoo et al. (Fig. S4, Table S1†),[27] which comprise Cu(L1) layers

either perfectly offset with PW units in the centre of neighbouring pores or imperfectly offset. The desolvated phase has also been documented in the PXRD patterns reported by Kanoo et al. and provides a good match with the desolvated MOF and nanosheets obtained in this work, although a crystal structure was not reported.[27]

Cu(L2) forms as a dark blue powder from both salts. In this instance, both the MOFs formed from the acetate and nitrate salts were found to be ~90% solvated through microanalysis and ^{1}H NMR studies. The PXRD pattern of this material can be Pawley fitted to unit cell dimensions that closely match a layered Zn_2-PW structure previously reported by Kongshaug and Fjellvåg (Fig. S5, Table S2†),[32] consistent with those observed by Gascon et al.,[34] in which Cu(L2) adjacent layers are offset. There is a phase change observed upon desolvation via acetonitrile exchange, as indicated by the PXRD pattern, the Pawley fitting of which yields unit cell parameters consistent with a Cu_2-PW structure also reported by Kongshaug and Fjellvåg.[32]

Cu(L3) forms as a light blue powder on synthesis from both salts and has no DMF present. No single crystal data for this system have been reported and our attempts to grow single crystals were unsuccessful. However, a SURMOF system demonstrated by Wöll and co-workers shows powder patterns consistent with those obtained in this study. In their modelling, this layered system has highly symmetrical $P4$-type stacking, in which each Cu_2-PW stacks directly above and below those in adjacent layers.[33] Microanalysis, ^{1}H NMR, and Fourier-transform infrared (FT-IR) spectra confirm the absence of DMF and indicate the presence of one molecule of water per Cu(L3) unit, which likely occupy the pores of the framework to give four molecules of water per pore. In contrast to the other two materials, no significant structural changes were observed following exfoliation or desolvation.

A substantial difference in the rate of crystal growth was observed between the reactions to form the layered MOFs from the two different salts. Use of the acetate salt led to the precipitation of microcrystalline powders almost immediately at room temperature, prior to heating, whereas when the nitrate salt was used precipitate formation occurred only upon heating (Fig. S7†). As shown in Fig. 2, scanning electron microscopy (SEM) images of all MOFs synthesised from the nitrate salt showed particles approximately 1–15 μm in size with clearly layered morphologies. This layering is also observed in the SEM images of the desolvated forms of these systems (Fig. S19†), which also show similar particle size ranges. In contrast, images of the systems formed from the acetate source showed only poorly-defined aggregates of <1 μm size, and no clearly defined layering was observed in these samples. Such aggregates have been observed in previous reports of copper-based MOF systems prepared from the acetate salt.[30,35,36]

We attribute this difference in particle size and morphology to three different factors: (1) prearrangement of the Cu^{2+} ions in the PW structure with the acetate anion leads to an accelerated rate of reaction with the linker ligands and consequently
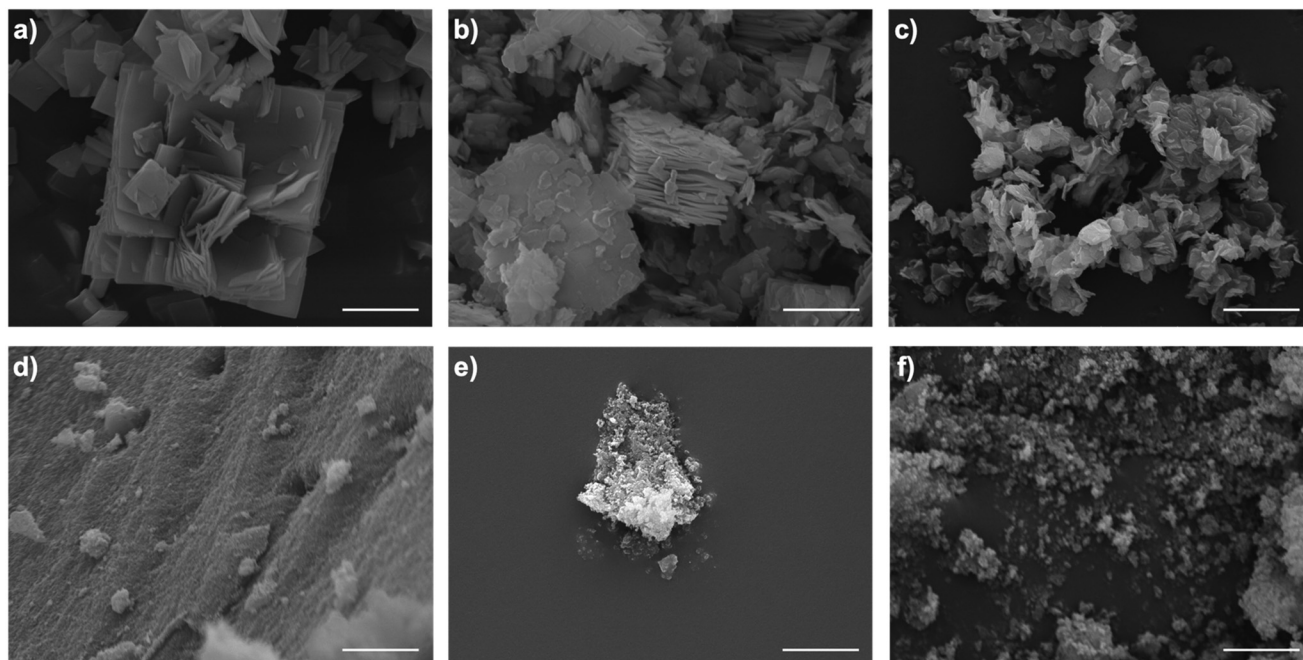
Fig. 2 SEM images of the layered MOFs (a) Cu(L1), (b) Cu(L2) and (c) Cu(L3) formed from the nitrate salt, and (d) Cu(L1), (e) Cu(L2), and (f) Cu(L3) formed from the acetate salt. Supplementary SEM images are provided in Fig. S16–S18.† All scale bars represent 5 μm.

faster crystallisation into smaller particles,[37] (2) the acetate ions facilitate faster deprotonation of the dissolved linker precursors also leading to faster crystallisation, and (3) the acetate acts as a monotopic crystal size modulator, restricting growth in the lateral dimensions.[38–41] This is further evidenced by ^{1}H NMR spectroscopy of the digested MOFs, (Fig. S8–S13†) which shows 3–5% incorporation of acetate into each of the MOF structures.

Liquid exfoliation to form MONs

The prominent difference in particle size between both series of layered MOFs serves as an ideal starting point to investigate the effect of the precursor system size on its liquid exfoliation into MONs. In order to investigate these effects, all layered MOFs were subjected to the same exfoliation procedure that we have previously reported, in which soft high-frequency ultrasound is used to reduce fragmentation, whilst samples are stirred to minimize hot-spots and aid reproducibility. Acetonitrile was chosen as the exfoliation solvent, as our previous work has shown it to be an effective candidate for related copper benzenedicarboxylate-based systems.[22,42,43] MOF samples (5 mg) were suspended in acetonitrile (6 mL) in a sealed vial and subjected to ultrasound at 80 kHz for 12 hours at 15–18 °C temperatures. Each sample was then centrifuged at 362g (1500 rpm) for 1 hour to remove the bulk unexfoliated material, leaving the nanosheets in suspension.

The suspension concentrations of both series were demonstrably different even from naked eye observations. The MON suspensions obtained from exfoliation of the acetate series were substantially more intense in colour, as shown in

Fig. S21.† This is confirmed by Tyndall scattering observations, in which scattering is much stronger for the acetate series, suggesting a higher concentration of colloidal material in suspension. UV-visible spectroscopy was used to determine the obtained concentrations, which corroborated this qualitative evidence. As presented in detail in Table S4,† the concentrations of the series prepared from nitrate salts, 0.05–0.1 mg mL^{-1}, are significantly reduced compared to those prepared from acetate salts, which give high yields of 0.6–0.7 mg mL^{-1}. All MON samples are colloidally stable for at least 3 days. However, after this time MON suspensions obtained from the nitrate series begin to precipitate (Fig. S22†), whereas those from the acetate series remain stable in suspension for at least a month. We attribute this difference in the colloidal stability to the enhanced surface areas of the larger aspect ratio nanosheets, leading to a great number of van der Waals interactions between adjacent particles and thus to aggregation and subsequent precipitation.[26]

The PXRD patterns of each system post-exfoliation indicate a phase change to the desolvated forms in all systems. We have observed this phenomenon in multiple previous reports in which we have performed liquid exfoliation of DMF-solvated MOFs using excess acetonitrile. Acetonitrile displaces DMF from the PW axial sites, but does not remain coordinated once the material is dried. This is further evidenced by ^{1}H NMR spectra of the bulk material obtained after exfoliation, which indicate full desolvation in each system (Fig. S29–S31†).

Atomic force microscopy (AFM) topographical imaging of all samples shows distinct trends in the morphology for both series, with size distribution data for all samples being pre-

Table 1 Summary of the statistical size distribution data of MONs obtained from the exfoliation of the MOF isoreticular series synthesised from nitrate and acetate salts. Additional AFM images used for size distribution analyses can be seen in Fig. S31–S33†

	Cu(1,4-NDC)		Cu(2,6-NDC)		Cu(BPDC)	
	NO_3^-	AcO^-	NO_3^-	AcO^-	NO_3^-	AcO^-
$\bar{x}$ T ± SD/nm	0.80 ± 0.04	77 ± 54	0.80 ± 0.05	101 ± 70	0.80 ± 0.03	71 ± 62
$\bar{x}$ LD ± SD/nm	220 ± 172	374 ± 152	400 ± 335	414 ± 128	821 ± 441	183 ± 97
$\bar{x}$ AR ± SD/nm	270 ± 210	7.1 ± 4.4	502 ± 437	5.4 ± 3.1	1020 ± 550	3.6 ± 1.9

LD = largest lateral dimension, T = thickness, AR = aspect ratio, $\bar{x}$ = mean average value of the parameter and SD = standard deviation. Mean aspect ratios were determined for individual particles.
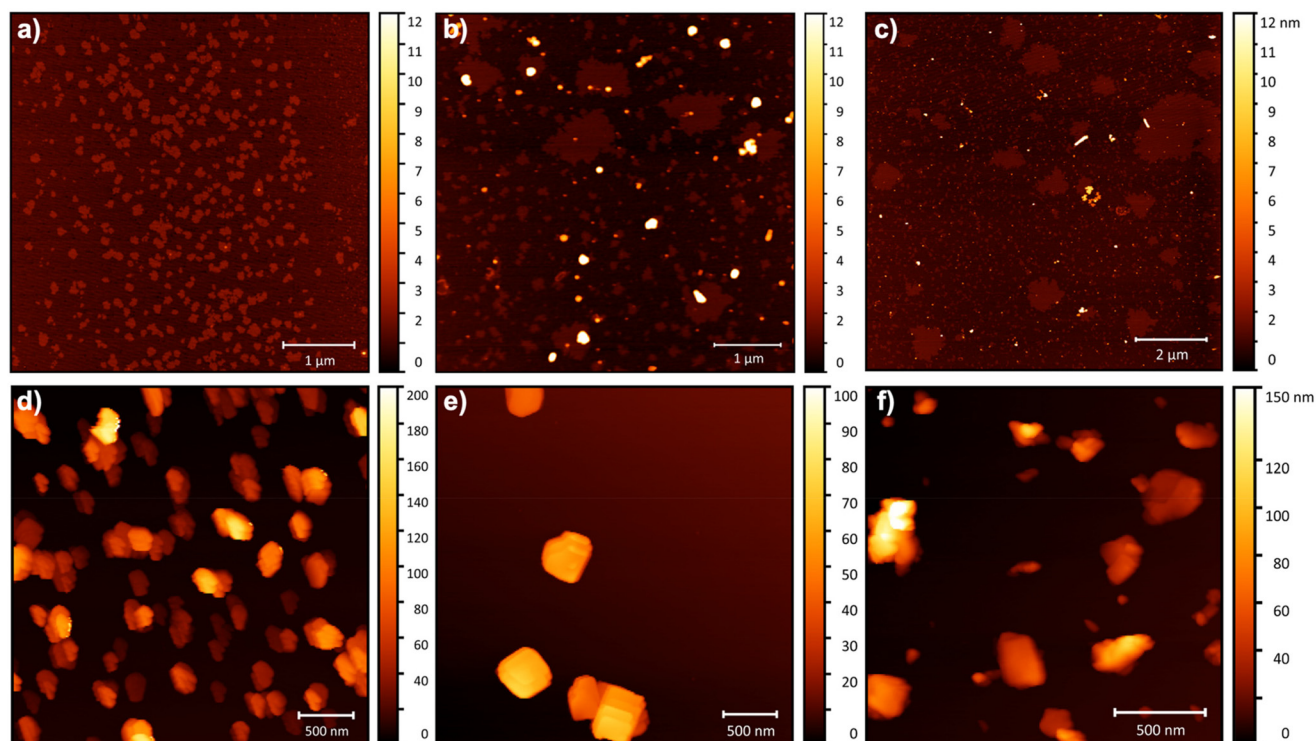

Fig. 3 AFM topographical images of MONs obtained from the liquid exfoliation of layered MOFs (a) Cu(L1), (b) Cu(L2) and (c) Cu(L3) prepared from the nitrate salt and (d) Cu(L1), (e) Cu(L2) and (f) Cu(L3) prepared from the acetate salt. Additional images and height profiles are provided in Fig. S32, S34 and S35–S50† respectively.

sented in detail in Table 1. As shown in Fig. 3, MONs obtained from the nitrate series are consistently ultrathin, down to monolayer thicknesses of ~0.8 nm (Fig. S41†). In contrast, these images indicate that all MONs in the acetate series were clearly multilayer with average thicknesses between 71 and 101 nm. Although there is no clear trend in the lateral size distribution between the two series, the aspect ratios of the nanosheets obtained from the nitrate salt are orders of magnitude larger, owing to their ultrathin thicknesses.

The key variable between the two series is the initial particle sizes of the layered MOFs exfoliated to obtain these nanosheets. As such, we attribute this difference in nanosheet thicknesses to the difference in the particle sizes of the precursor MOFs. SEM imaging of the bulk material removed by centrifugation post-exfoliation for the nitrate series continues to

show particles of micrometre size with defined layers, despite ultrasonication for extensive periods of time (Fig. S44–S46†). This may suggest that the larger particles of the nitrate series preferentially delaminate into ultrathin nanosheets, fragmenting largely only once dispersed. In contrast, the smaller particles of the acetate series disperse much more easily, meaning ultrasound forces induce delamination and fragmentation simultaneously. This difference in the precursor MOF particle size could also explain the difference in concentration obtained from each series, with the smaller acetate systems dispersing more easily, leading to higher exfoliation yields.

Within the series of nanosheets with a monolayer thickness that are produced from the nitrate salt, the lateral sizes and aspect ratios appear to increase with lengthening of the ligand (Fig. 4). Exfoliation of Cu(L1) clearly gives smaller nanosheets
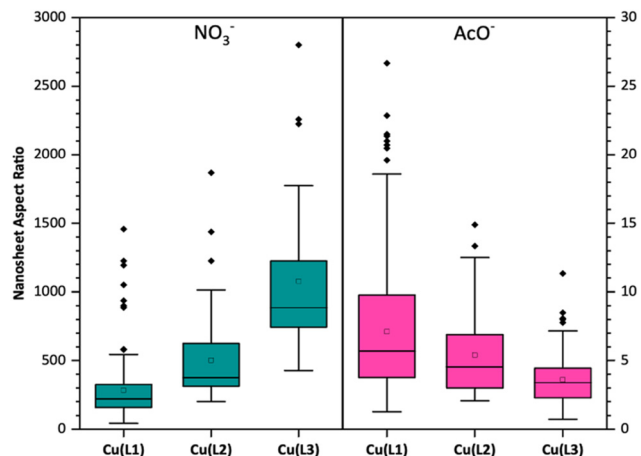
Fig. 4 Box plots of Cu(L1), Cu(L2), and Cu(L3) MON aspect ratios for nanosheets prepared from the nitrate salt (green) and acetate salt (pink). Note the different scales for the nanosheet aspect ratio on the left and right hand sides.

220 ± 172 nm wide, whereas Cu(L3) yields much larger nanosheets with average lateral dimensions of 821 ± 441 nm. Cu(L2) appears to give a mixture of both small and large nanosheets, resulting in average widths of intermediate value at 400 ± 335 nm. This is tentatively attributed to the higher density of metal nodes associated with shorter linkers, which are the most likely fragmentation sites. Interestingly, the nanosheets with the longer linkers (L2 and L3) have highly irregular shapes, a phenomenon which we have previously observed in similar ultrathin supramolecular systems.[25,44] In contrast, no clear trend in thicknesses or lateral size distributions was observed within the acetate series by AFM, with a significant degree of overlap being observed for the aspect ratio measurements.

Due to the low concentrations of the MON suspensions obtained from the nitrate series, dynamic light scattering (DLS) data could not be obtained for these systems. However, DLS measurements of the MON suspensions obtained from the acetate salts corroborate the trend in the lateral size distributions obtained from the AFM of each system, with number average diameters of 121 nm (Cu(L1)), 234 nm (Cu(L2)), and 56 nm (Cu(L3)) (Fig. S42 and S43†). As noted in previous reports, DLS measurements underestimate the lateral dimensions of nanosheets with respect to AFM, due to the assumption of spherical particles made in using the Stokes–Einstein equation.

Conclusions

Understanding how to control the dimensions of nanosheets obtained through liquid exfoliation is a key challenge in realising their use across a range of applications that rely on their high surface areas and exposed active sites. In this study, we therefore developed an isoreticular series of layered Cu$_2$-PW

MOFs incorporating three different lengths of the dicarboxylate ligand and formed from two different copper salts. The samples were subjected to identical ultrasonic liquid exfoliation protocols and the structure and properties of the resulting particles were analysed. The use of more soluble nitrate salts produced large crystals which exfoliated well to form monolayer nanosheets with large lateral dimensions, although only low concentrations of the material were isolated. In contrast, more rapid crystal growth in the material synthesised using the acetate salts produced smaller crystallites which exfoliated to produce much higher concentrations of the material in suspension, but these were found to be a few layers thick with smaller lateral dimensions. The initial particle size of the MOF therefore appears to be key to determining the aspect ratio of the nanosheets formed, with larger particles predominantly undergoing delamination, and smaller ones undergoing greater fragmentation. Furthermore, the use of longer linker ligands resulted in increased aspect ratios within the consistently monolayer nitrate series which are attributed to the reduced density of metal nodes when longer ligands are present. We anticipate that these insights from this systematic study will provide useful guidelines into the design of improved MON systems with ultrahigh surface areas.

Experimental

Further details on materials, reagents, equipment and characterisation methods are available in the ESI.†

Layered MOF syntheses

To prepare each layered MOF, the copper salt of choice (0.125 mmol) and the dicarboxylic acid ligand precursor (0.131 mmol) were each dissolved in DMF (5 mL) and then combined in reaction vials with Teflon-lined caps. The reaction mixtures were placed in a reaction oven and heated to 110 °C at a rate of 1 °C min^{-1}, and then maintained at this temperature for 18 hours, after which they were cooled to room temperature at a rate of 0.1 °C min^{-1}. The samples were then transferred to polypropylene centrifuge tubes and centrifuged at 3258g (4500 rpm, 5 min), then the supernatant was removed. The samples were then washed with DMF (3 × 30 mL, 4500 rpm, 30 min) and diethyl ether (2 × 25 mL, 4500 rpm, 2 min), before being left to dry in air and then in a vacuum oven (60 °C, 4 hours), affording each MOF as a microcrystalline powder.

Layered MOF desolvation

The layered MOFs (30 mg) were desolvated through suspension in acetonitrile (10 mL) followed by stirring for 3 hours. The samples were centrifuged at 3258g (4500 rpm, 5 min), after which the solvent was decanted and replaced with fresh solvent. This process was repeated 5 times, followed by the removal of excess solvent by washing with diethyl ether (2 × 5 mL) and drying in vacuo.

Liquid exfoliation

Samples of layered MOF (5 mg) were suspended in acetonitrile (6 mL) in reaction vials with Teflon-lined caps. The samples were then sonicated at 80 kHz for 12 hours at 100% power, at a temperature <18 °C and with stirring of the vials to prevent hot spots. Sonication was followed by centrifugation for 1 hour at 362g (1500 rpm) to remove the unexfoliated material, followed by separation of the supernatant to yield suspensions of MONs.

Author contributions

J. N., D. J. A., and G. D. synthesised and characterised the layered MOFs. T. M. R. performed all Pawley refinement analysis. M. H. performed all SEM imaging. J. N. and G. D. prepared and characterised all MONs. J. N. drafted the manuscript and the ESI,† and created all figures. L. B. and J. A. F. provided supervision. J. A. F. conceived the project and edited the manuscript.

Data availability

The data supporting this article have been included as part of the ESI.†

Conflicts of interest

There are no conflicts to declare.

Acknowledgements

References

1 M. J. Allen, V. C. Tung and R. B. Kaner, *Chem. Rev.*, 2010, **110**, 132–145.

2 M. Zhao, Y. Huang, Y. Peng, Z. Huang and Q. Ma, *Chem. Soc. Rev.*, 2018, **47**, 6267–6295.

3 D. J. Ashworth and J. A. Foster, *J. Mater. Chem. A*, 2018, **6**, 16292–16307.

4 G. R. Bhimanapati, Z. Lin, V. Meunier, Y. Jung, J. Cha, S. Das, D. Xiao, Y. Son, M. S. Strano, V. R. Cooper, L. Liang, S. G. Louie, E. Ringe, W. Zhou, S. S. Kim, R. R. Naik, B. G. Sumpter, H. Terrones, F. Xia, Y. Wang, J. Zhu, D. Akinwande, N. Alem, J. A. Schuller, R. E. Schaak, M. Terrones and J. A. Robinson, *ACS Nano*, 2015, **9**, 11509–11539.

5 J. Nicks, K. Sasitharan, R. R. R. Prasad, D. J. Ashworth and J. A. Foster, *Adv. Funct. Mater.*, 2021, **31**, 2103723.

6 P. Z. Moghadam, A. Li, X.-W. Liu, R. Bueno-Perez, S.-D. Wang, S. B. Wiggin, P. A. Wood and D. Fairen-Jimenez, *Chem. Sci.*, 2020, **11**, 8373–8387.

7 G. Chakraborty, I.-H. Park, R. Medishetty and J. J. Vittal, *Chem. Rev.*, 2021, **121**, 3751–3891.

8 J. N. Coleman, M. Lotya, A. O. Neill, S. D. Bergin, P. J. King, U. Khan, K. Young, A. Gaucher, S. De, R. J. Smith, I. V. Shvets, S. K. Arora, G. Stanton, H. Kim, K. Lee, G. T. Kim, G. S. Duesberg, T. Hallam, J. J. Boland, J. J. Wang, J. F. Donegan, J. C. Grunlan, G. Moriarty, A. Shmeliov, R. J. Nicholls, J. M. Perkins, E. M. Grieveson, K. Theuwissen, D. W. Mccomb, P. D. Nellist and V. Nicolosi, *Science*, 2011, **331**, 568–572.

9 H. Tao, Y. Zhang, Y. Gao, Z. Sun, C. Yan and J. Texter, *Phys. Chem. Chem. Phys.*, 2017, **19**, 921–960.

10 Z. Li, R. J. Young, C. Backes, W. Zhao, X. Zhang, A. A. Zhukov, E. Tillotson, A. P. Conlan, F. Ding, S. J. Haigh, K. S. Novoselov and J. N. Coleman, *ACS Nano*, 2020, **14**, 10976–10985.

11 A. Ciesielski and P. Samorì, *Chem. Soc. Rev.*, 2014, **43**, 381–398.

12 J. Shen, Y. He, J. Wu, C. Gao, K. Keyshar, X. Zhang, Y. Yang, M. Ye, R. Vajtai, J. Lou and P. M. Ajayan, *Nano Lett.*, 2015, **15**, 5449–5454.

13 C. Backes, T. M. Higgins, A. Kelly, C. Boland, A. Harvey, D. Hanlon and J. N. Coleman, *Chem. Mater.*, 2017, **29**, 243–255.

14 M. Zhao, Y. Huang, Y. Peng, Z. Huang, Q. Ma and H. Zhang, *Chem. Soc. Rev.*, 2018, **47**, 6267–6295.

15 S. Jindal, V. K. Maka, G. Anjum and J. N. Moorthy, *ACS Appl. Nano Mater.*, 2021, **4**, 449–458.

16 P. Chandrasekhar, A. Mukhopadhyay, G. Savitha and J. N. Moorthy, *J. Mater. Chem. A*, 2017, **5**, 5402–5412.

17 Y. Peng, Y. Li, B. Yujie, H. Jin, W. Jiao, X. Liu and W. Yang, *Science*, 2014, **346**, 1356–1359.

18 D. Liu, B. Liu, C. Wang, W. Jin, Q. Zha, G. Shi, D. Wang and X. Sang, *ACS Sustainable Chem. Eng.*, 2020, **8**, 2167–2175.

19 X. Sang, D. Liu, J. Song, C. Wang, X. Nie, G. Shi, X. Xia, C. Ni and D. Wang, *Ultrason. Sonochem.*, 2021, **72**, 105461.

20 H. Zhou, L. Zhang, G. Wang, Y. Zhang, X. Wang, M. Li, F. Fan, Y. Li, T. Wang, X. Zhang and Y. Fu, *ACS Appl. Mater. Interfaces*, 2021, **13**, 39755–39762.

21 J. Gosch, K. Synnatschke, N. Stock and C. Backes, *Chem. Commun.*, 2023, **59**, 55.

22 D. J. Ashworth, A. Cooper, M. Trueman, R. W. M. Al-Saedi, L. D. Smith, A. J. H. M. Meijer and J. A. Foster, *Chem. – Eur. J.*, 2018, **24**, 17986–17996.

23 D. J. Ashworth and J. A. Foster, *Nanoscale*, 2020, **12**, 7986–7994.

24 D. J. Ashworth, T. M. Roseveare, A. Schneemann, M. Flint, I. D. Bernáldes, P. Vervoorts, R. A. Fischer, L. Brammer and J. A. Foster, *Inorg. Chem.*, 2019, **58**, 10837–10845.

25 J. Nicks, J. Zhang and J. A. Foster, *Chem. Commun.*, 2019, **55**, 8788–8791.

26 J. Zhan, Z. Lei and Y. Zhang, *Chem*, 2022, **8**, 947–979.

27 P. Kanoo, K. L. Gurunatha and T. K. Maji, *J. Mater. Chem.*, 2010, **20**, 1322.

28 M. Eddaoudi, J. Kim, D. Vodak, A. Sudik, J. Wachter, M. O'Keeffe and O. M. Yaghi, *Proc. Natl. Acad. Sci. U. S. A.*, 2002, **99**, 4900–4904.

29 X. Wang, D. Zhu, Y. Xu, J. Yang, X. Shen, J. Zhou, N. Fei, X. Ke and L. Peng, *Cryst. Growth Des.*, 2010, **10**(2), 887–894.

30 J. Nicks and J. A. Foster, *Nanoscale*, 2022, **14**, 6220–6227.

31 F. Shahangi Shirazi and K. Akhbari, *Inorg. Chim. Acta*, 2015, **436**, 1–6.

32 K. O. Kongshaug and H. Fjellvåg, *J. Solid State Chem.*, 2002, **166**, 213–218.

33 J. Liu, B. Lukose, O. Shekhah, H. K. Arslan, P. Weidler, H. Gliemann, S. Bräse, S. Grosjean, A. Godt, X. Feng, K. Müllen, I. B. Magdau, T. Heine and C. Wöll, *Sci. Rep.*, 2012, **2**, 1–5.

34 T. Rodenas, I. Luz, G. Prieto, B. Seoane, H. Miro, A. Corma, F. Kapteijn, F. X. Llabrés i Xamena and J. Gascon, *Nat. Mater.*, 2014, **14**, 48–55.

35 K. Y. A. Lin, H. Yang, C. Petit and F. K. Hsu, *Chem. Eng. J.*, 2014, **249**, 293–301.

36 J. G. Flores, E. Sánchez-González, A. Gutiérrez-Alejandre, J. Aguilar-Pliego, A. Martínez, T. Jurado-Vázquez, E. Lima, E. González-Zamora, M. Díaz-García, M. Sánchez-Sánchez and I. A. Ibarra, *Dalton Trans.*, 2018, **47**, 4639–4645.

37 R. Ameloot, F. Vermoortele, W. Vanhove, M. B. J. Roeffaers, B. F. Sels and D. E. De Vos, *Nat. Chem.*, 2011, **3**, 382–387.

38 R. S. Forgan, *Chem. Sci.*, 2020, **11**, 4546–4562.

39 M. Pham, G. Vuong, F.-G. Fontaine and T. Do, *Cryst. Growth Des.*, 2012, **12**, 3091–3095.

40 K. A. S. Usman, J. W. Maina, S. Seyedin, M. T. Conato, L. M. Payawan, L. F. Dumée and J. M. Razal, *NPG Asia Mater.*, 2020, **12**, 1–18.

41 C. R. Marshall, S. A. Staudhammer and C. K. Brozek, *Chem. Sci.*, 2019, **10**, 9396–9408.

42 J. A. Foster, S. Henke, A. Schneemann, R. A. Fischer and A. K. Cheetham, *Chem. Commun.*, 2016, **52**, 10474–10477.

43 J. Nicks, J. Zhang and J. A. Foster, *Chem. Commun.*, 2019, **55**, 8788–8791.

44 J. Nicks and J. A. Foster, *Nanoscale*, 2022, **14**, 6220.